

pubs.acs.org/cm Article

Strong, Ductile MOF-Poly(urethane urea) Composites

Joseph M. Palomba, David M. Wirth, Jin Yeong Kim, Mark Kalaj, Evan M. Clarke, Gregory W. Peterson, Jonathan K. Pokorski, and Seth M. Cohen*



Cite This: Chem. Mater. 2021. 33, 3164-3171



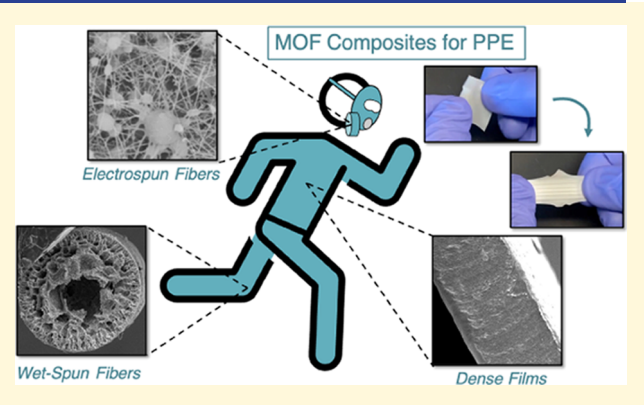
ACCESS

Metrics & More

Article Recommendations

Supporting Information

ABSTRACT: Metal—organic framework (MOF)—polymer hybrid materials have been investigated for use in personal protective equipment (PPE) for combating chemical threats. However, few of these composite materials have demonstrated the desired processability or balance of strength and ductility suitable for modern textiles. In this work, a poly(urethane urea) (PUU) polymer was synthesized to mimic solution-processable spandex for MOF composites that have combined advantages for both the force the composite can withstand (strength) and the ability of the material to deform under strain (ductility). UiO-66/PUU mixed matrix membranes (MMMs) with up to 50 wt % UiO-66 MOF showed both high strength and ductility. UiO-66 and UiO-66-NH2 MMMs with PUU mechanically outperformed previously studied 50 wt % MOF/poly(vinylidene



difluoride) (PVDF) MMMs. Testing of MMMs against the chemical warfare agent simulant dimethyl-4-nitrophenylphosphate (DMNP) revealed that the polymer plays an important role, with UiO-66-NH₂/PUU MMM showing the fastest hydrolysis rate. Ductile fibers of 50 wt % UiO-66 and UiO-66-NH₂ PUU composites were successfully prepared and showed remarkable handling properties and activity toward DMNP hydrolysis with 50 wt % UiO-66-NH₂/PUU fibers performing better than any of the MMMs tested. These MOF—polymer composites could also be electrospun into nanofiber mats, which further illustrates the diverse range of processing techniques available for these materials.

■ INTRODUCTION

Metal—organic frameworks (MOFs) have been explored for the next generation of sorbents and catalysts for personal protective equipment (PPE).^{1–3} MOFs are two- and three-dimensional (3D), crystalline, porous solids that possess high surface areas (many >2000 m²/g) and tunable chemical functionalization.^{4,5} Several MOFs have been shown to absorb and break down toxic industrial chemicals (TICs) and chemical warfare agents (CWAs) more effectively than the state-of-the-art porous carbons used in conventional filter and PPE technologies.^{6,7} Compared to other materials, such as metal oxides,^{8,9} zeolites,¹⁰ and porous polymers,¹¹ MOFs provide the best broad-spectrum protection against a series of CWAs and TICs.^{6,7,12}

Most research has centered around Zr(IV)-based MOFs due to their high stability, versatile functionalization, and metal-catalyzed hydrolysis of organophosphorus nerve agents. $^{3,13-15}$ Specifically, Zr-MOF UiO-66 (UiO = University of Oslo, $Zr_6O_6(1,4$ -benzenedicarboxylate) $_6$) and its derivatives have been demonstrated as protective materials against NH $_3$, 16 Cl $_2$, 17 and a variety of nerve agents. 18 However, MOFs like UiO-66 are synthesized as free-flowing powders that require strategies to effectively integrate them into PPE applications. The lack of mechanically robust composites is a bottleneck for the implementation of MOFs and is among the most

significant limitations for using MOFs to replace porous carbons used in $\mbox{\rm PPE.}^{1,7}$

Polymer composites of MOFs have been explored as more suitable form factors for adapting MOFs to PPE such as uniforms, protective suits, masks, gloves, and boots. 1,19-23 MOF composites that protect against chemical threats have been prepared using atomic layer deposition-coated (ALD) nanofibers, 20,24 mixed matrix membranes (MMMs), 21,25,26 electrospun nanofibers, 23,27,28 and postsynthetic polymerization (PSP). 19 However, many of these composites, particularly those with the highest TIC uptake or best CWA degradation activity, are not mechanically robust. Some key metrics for evaluating PPE composites are yield strength—the maximum stress a material can withstand without undergoing plastic deformation—and ductility—the ability of a material to plastically deform without breaking, typically measured by percent elongation at failure. Strong, ductile MOF-polymer composites of considerable loading (>30 wt % MOF) have yet

Received: December 22, 2020 Revised: April 6, 2021 Published: April 23, 2021





to be realized.²⁹⁻³¹ In one study, the combination of two brittle polymers, Polymer of Intrinsic Microporosity-1 (PIM-1) and polyacrylonitrile (PAN), with UiO-66-NH2 resulted in a material with an elongation at break of 34% and an ultimate tensile strength of 0.72 MPa.²⁷ This material has accessible porosity but does not have the toughness necessary for the mechanical challenges expected for protective textiles. An example of a composite with improved mechanical properties uses modified HKUST-1 in 20 wt % MOF poly(styrene-blockethylene-ran-butylene-block-styrene) (SEBS) that shows an elongation at break of 550% and an ultimate tensile strength of 8.5 MPa.³² While these materials have good mechanical properties at low MOF loadings, microscopy shows gaps between the MOF and the polymer that would make higher loading composites much more brittle.³² To overcome these limitations, the matrix polymer must be selected to have sufficient ductility and also appropriate interactions with MOF particles that balance a close interface without pore blockage. The goal of the study presented here is to create a MOFpolymer composite that maximizes MOF performance balanced with mechanical properties.

Poly(urethane urea)s (PUUs) combine the ductility of polyurethanes and long polyol chains with strength resulting from interchain hydrogen bonding from urea functional groups. For this reason, PUUs are the most common synthetic polymers in flexible athletic apparel, commonly known as spandex or elastane.³³ In this work, PUU (Figure 1) was

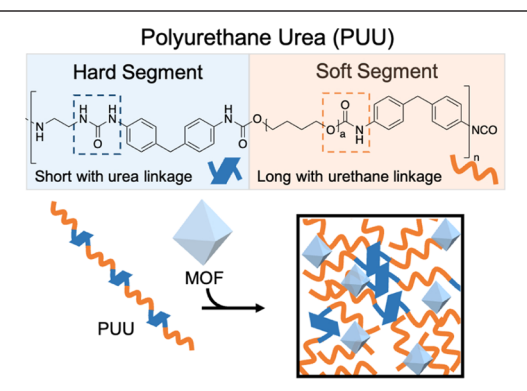


Figure 1. Top: general overview of the poly(urethane urea) (PUU) polymer. Bottom: scheme representing the MOF–PUU composites.

synthesized and MOF-polymer composites were made with various MOF loadings. UiO-66 was used as a model system and MMMs of PUU were fabricated successfully with up to 50 wt % MOF. These materials displayed excellent mechanical properties and maintained a high degree of flexibility with added strength from the MOFs that act as both an active material and a filler. The PUU composites were tested for CWA simulant degradation and compared to equivalent MMMs made with poly(vinylidene difluoride) (PVDF). PUU composite fibers were spun with UiO-66 and UiO-66-NH₂ at 50 wt % and despite the high MOF content could be easily handled while also showing activity toward CWA simulant degradation. Using electrospinning, 20 wt % MOF/ PUU nanofiber mats were made with good dispersions of both UiO-66 and UiO-66-NH2 to further showcase the ability to process these composites into multiple form factors. These MOF/PUU composites provide an adaptable platform for functional PPE.

METHOD SECTION

Synthesis of the Poly(urethane urea) Polymer. Polytetrahydrofuran (polyTHF, $M_{\rm w}$ = 2000 g/mol, 10.0 g, 5.00 mmol) was added as a solid to a 250 mL round-bottom flask, dissolved in N,N-dimethylacetamide (DMAC, dried over molecular sieves) (10.0 g) and stirred under an Ar atmosphere at 80 °C for 10 min. To this, 4,4'-methylene diphenyl diisocyanate (MDI, 2.55 mg, 10.0 mmol) was added in 5.0 mL of DMAC and stirred (>500 rpm) for an additional 10 min. To catalyze the reaction, 2.50 mL of a 0.1 wt % stannous octoate (5.35 μ mol) solution in CHCl₃ was added and the reaction was stirred at 80 °C for 3 h. If necessary, DMAC (5-10 mL) was added to dilute the solution to allow for continuous stirring. After 3 h, the solution (termed the "prepolymer") was diluted with 20 mL of DMAC and then ethylene diamine (334 μ L, 5.00 mmol) in 10 mL of DMAC was added to the reaction mixture. Polymerization occurred upon addition and was complete in <20 min. Note, depending on the efficiency of stirring, more DMAC (10-50 mL) may be required to solubilize the final polymer. The final polymer was precipitated in 1 L of EtOH and washed with EtOH (2 × 800 mL) and dried at 60 °C for 12 h under vacuum.

MOF/PUU MMM Fabrication. UiO-66 and UiO-66-NH₂ were synthesized according to literature procedures (see the Supporting Information). The MOF (100-300 mg) was dispersed in an ethyl acetate solution (~8 mL) via sonication. Note, preparation of the MOF materials for making highquality MMMs was achieved by grinding the MOF powders with a mortar and pestle followed by sonication of the ground samples. The ground MOF samples were transferred to a glass vial that was placed in the center of a Branson 2800 sonicator bath and sonicated at full power for 30 min. A 15 wt % PUU solution in DMAC was added to yield corresponding wt % MMMs (e.g., for a 50 wt % UiO-66 MMM, 150 mg of UiO-66 was combined with 1.0 g of the polymer solution). The MOF and polymer solutions were thoroughly mixed in a sonication bath for 1 h. The resulting "ink" was then subjected to rotary evaporation to remove the ethyl acetate and concentrated to a honey-like viscosity. The MOF-polymer solution was then transferred to a substrate, either aluminum foil or glass, and then cast using a drawdown method with a doctor blade set to a height of 950 μ m at a speed of 25 mm/s. The cast films were then cured at 65 °C in a preheated oven under a thin-neck glass funnel for 12 h. After cooling, ~2 mL of iPrOH was dropped on the films to induce swelling and the films were delaminated with tweezers and allowed to dry.

Tensile Testing. Tensile measurements were carried out on 15 mm \times 40 mm rectangular films with the thickness and the width recorded in the center of the film. Sample thicknesses were measured using a Mitutoyo digital micrometer (0–25 mm range, 0.001 mm resolution) for films (\sim 60 to 100 μ m) and using cross-sectional images from a scanning electron microscope (SEM) for fibers (\sim 300 μ m). The samples (3–4 segments from the same film) were acquired using a CellScale UniVert mechanical testing apparatus with a 100 N load cell for films and a 10 N load cell for fibers at an extension rate of 0.17 mm/s, a preload of 0.2 N, and a sampling rate of 15 Hz to generate stress—strain curves. Yield strength, ultimate tensile strength, elastic modulus, elongation at break, and toughness were calculated using MS Excel (see Supporting Information for details).

Screening of MMMs for DMNP Hydrolysis. Membranes (\sim 12 mm \times 8 mm, prepared and measured in triplicate for each sample) were inserted into 3D printed plastic holders³ and placed in individual wells of an Olympus Plastics clear, flatbottom 24-well assay plate. To avoid beam blockage, a small rubber o-ring was used to keep the membrane in place along the wall of the well. A buffer solution (2 mL of 20 mM N-ethylmorpholine, pH = 8.0) was added to each well. A solution of dimethyl-4-nitrophenylphosphate (DMNP, 20 μ L of 25 mM MeOH) was added and the appearance of p-nitrophenoxide was monitored at λ_{max} = 407 nm, every 12 s for 30 min. Slopes were calculated from the linear region of each plot (typically at 200–800 s) and normalized by the mass of the membrane.

MOF/PUU Fiber Spinning. Similar to the MMMs described above, 100–300 mg of the MOF was dispersed in an ethyl acetate solution (~8 mL) via sonication. A 15 wt % PUU solution in DMAC was added to yield corresponding wt % fibers. The resulting ink was then subjected to rotary evaporation to remove the ethyl acetate and concentrated to a honey-like viscosity. The MOF–polymer solution was then taken up in a 1 mL syringe fitted with a 0.9 mm × 100 mm, blunt tip needle and secured to a syringe pump. The end of the needle was bent slightly and immersed (~1 cm deep) in a 1 L water bath at room temperature. The syringe pump was set to 0.6 mL/h and the MOF–polymer solution was injected into the water bath, and the resulting fiber was collected by wrapping around a large beaker. The fibers were dried at 65 °C in a preheated oven for 12 h.

MOF/PUU Electrospinning. The MOF (120 mg) was dispersed in 5 mL of DMF in a 20 mL scintillation vial and sonicated for 5 min using a probe sonicator. Next, PUU (500 mg) was added to the vial, and the mixture was magnetically stirred for 72 h. The solution was loaded into a 6 mL plastic syringe and transferred to a programmable floor-stand MSK-NFES-4 electrospinning unit (MTI Corporation). An electric field of 15 kV was applied across an ∼10 cm gap between a 20-gauge hypodermic needle and a stainless steel cylinder with an aluminum foil covering. Spinning was conducted at a solution flow rate of 1 mL/h for 15 min.

■ RESULTS AND DISCUSSION

MOF/PUU Composites. To emulate the mechanical properties of a commercial spandex polymer, solutionprocessable poly(urethane urea) (PUU) was synthesized. Narrow dispersity poly(tetrahydrofuran) with an $M_{\rm w}$ of 2000 g/mol (polyTHF₂₀₀₀, D = 1.34; Figure S1) was mixed with 4,4'-methylene diphenyl diisocyanate in a 1:2 ratio to afford a prepolymer (Figure 1 and Scheme S1). This prepolymer was then combined with 1 equiv of ethylenediamine to chain extend the prepolymer into the final block polymer. The final PUU polymer had a number average molecular weight (M_n) of ~80 000 g/mol relative to polystyrene standards (Scheme S1, Figure S1, and Table S1). The polymer formed rubbery masses, but could be dissolved in DMAC and cast to obtain clear, flexible films that were stretchable in all directions and could be extended multiple times their initial length (Figure S2 and Video S1).

Encouraged by the handling of the polymer films, MOF–polymer MMMs were made through casting UiO-66-based inks of various wt % (20–50 wt %). The MOF was well dispersed in the resulting translucent films (thickness of 60–100 μ m; Table S2) as evidenced by the scanning electron microscopy (SEM) images of 40 and 50 wt % MMMs and

PXRD of all MMMs (Figures 2 and S3-S5). Thermal gravimetric analysis (TGA) demonstrated that the 50 wt %

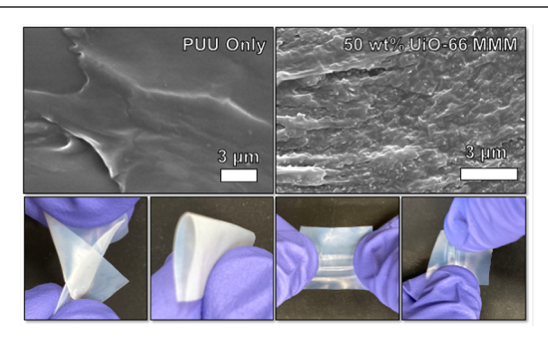


Figure 2. Top: cross-sectional SEM images of a pure PUU film (left) and 50 wt % UiO-66/PUU MMM (right). Bottom: photographs of 50 wt % UiO-66 being twisted, folded, and stretched.

MMM is stable up to at least 150 °C (Figures S6–S8). These materials could also be twisted, folded, or stretched in all directions without breaking or cracking, clearly adopting many mechanical properties of the parent polymer (Videos S2–S3).

Three ligand-modified UiO-66 MOFs were synthesized with 2-amino-1,4-benzenedicarboxylate (NH₂-bdc²⁻), 2-nitro-1,4-benzenedicarboxylate (NO₂-bdc²⁻), and naphthalene-1,4-dicarboxylic acid (Naph-bdc²⁻) to explore the compatibility of different MOFs with these composites. The incorporation of UiO-66-NH₂, UiO-66-NO₂, and UiO-66-Naph into 50 wt % MMMs was successful (Figures S2 and S9), showing that the PUU polymer is compatible with different MOFs.

The composites were found to have no Brunauer–Emmett–Teller (BET) surface area as prepared (Table S3), indicating that the MOF pores are not accessible to N_2 gas in these MMMs under these experimental conditions. It is possible that the pores of the MOF could be infiltrated partially by polyol chains as shown in other MOF–polymer systems, ³⁵ but the bulk of the phenyl rings on rigid blocks should prevent full polymer impregnation into the MOF pores. Another hypothesis to explain the lack of porosity of these composites is that at the subambient analysis conditions (77 K) of the gas sorption experiment, the polymer freezes, creating a gas-impermeable barrier on the MOF surface. In terms of PPE, the lack of N_2 uptake may preclude the use of these materials for respiratory applications (i.e., gas masks), but could make the composites useful for other PPE, such as in gloves or boots.

Strength and Flexibility of MOF/PUU Composites. To quantify the mechanical properties of the MOF/PUU composites, MMMs of 20, 30, 40, and 50 wt % UiO-66 were subjected to tensile testing. UiO-66-NH₂, which was found to possess a similar particle size to UiO-66 (UiO-66 = 128 \pm 29 nm vs UiO-66-NH₂ = 199 \pm 48 nm; Figure S10) was also tested in a 50 wt % MMM to compare their mechanical properties (Figures S2, S11, and S12). A pure PUU film and PVDF MMMs with 50 wt % UiO-66 or UiO-66-NH₂ were prepared as comparator materials (Figures S2 and S13 and Video S4). The ultimate tensile strength of the PVDF composite was previously reported, but ductility was not.

The properties for the pure PUU film agreed well with the literature values of high ductility that report elongations at break over 800%.³⁶ In fact, the films prepared in this study were so stretchable that they did not break inside the strain limits of the UniVert test stand, which has a practical maximum extension of <35 mm (Table 1 and Figures 3 and

Table 1. Mechanical Properties from Tensile Testing for PUU-Only Films and Selected MMMs^{a,b}

material	EAB (%)	yield str (MPa)	toughness (J/cm³)
PUU only	>1535	N/A^b	>47.8
20 wt % UiO-66/PUU	>1880	4.4 ± 0.3^{b}	>148.7
30 wt % UiO-66/PUU	>1610%	5.3 ± 0.4	>118.4
40 wt % UiO-66/PUU	479 ± 49	6.1 ± 0.1	37.4 ± 4.8
50 wt % UiO-66/PUU	146 ± 47	9.5 ± 0.5	16.7 ± 5.3
50 wt % UiO-66/PVDF	6 ± 4	6.9 ± 1.2	0.4 ± 0.2
50 wt % UiO-66-NH ₂ /PUU	129 ± 11	6.8 ± 0.7	10.0 ± 1.7
50 wt % UiO-66-NH ₂ /PVDF	4 ± 1	8.4 ± 4.0	0.2 ± 0.1
	1		

^aEAB = elongation at break and str = strength. ^bNo definitive plastic yield point observed.

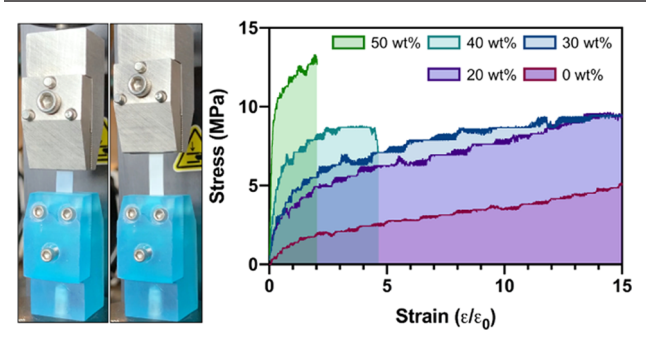


Figure 3. Left: photograph of tensile testing for the 50 wt % UiO-66/PUU MMM before the test and just before failure. Right: results of tensile testing for the PUU film (0 wt %) and UiO-66/PUU MMMs (20–50 wt %).

S14). In addition, films returned to their original size upon relaxation, as expected for an elastomer. The 50% UiO-66/PVDF and 50 wt % UiO-66-NH₂/PVDF MMMs showed higher ultimate tensile strengths (8.2 and 10.0, respectively) but less than 6% elongation at break (Figure 4 and Table S2).

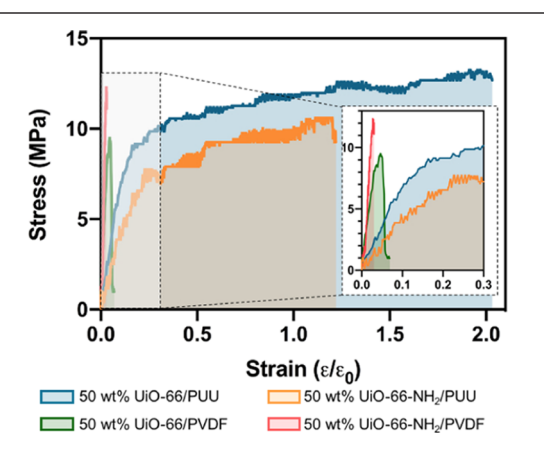


Figure 4. Results of tensile testing for 50 wt % MOF MMMs of PUU and PVDF with a low-strain region $(0-0.3 \ \varepsilon/\varepsilon_0)$ expanded in the inset.

The strength of the PVDF composites is on the order of PPE polymers used in nitrile or butyl protective gloves (22.7 and 9.1 MPa, respectively).^{37,38} However, PPE gloves require high ductility, as shown by nitrile and butyl materials also having elongations at break over 550%.^{37,38}

Using the flexible PUU polymer yielded very ductile MOF composite materials. The 20 and 30 wt % UiO-66/PUU MMMs showed extremely high elongations and all tests resulted in elongations of break above 1500% or no break at all

within the limits of the test (Figure 3 and Table S2). Higher weight loadings of UiO-66 in 40 and 50 wt % MMMs showed lower elongations at break, as expected, because of the addition of the filler to the polymer (Figure 3 and Table 1). However, 50 wt % UiO-66/PUU still showed an average elongation at break of 146% and a toughness (the ability of a material to absorb energy per unit volume as quantified by the area under the stress—strain curve) of 16.7 J/cm³ (Figures 3 and 4 and Table 1). The yield strength of the 50 wt % MOF MMMs were all between 6.8 and 9.5 MPa, demonstrating that the PUU and PVDF composites could withstand a similar force before deformation (Figure 4).

The addition of the MOF to the PUU elastomer showed rigidification that increased the strength of the composite. There was a continuous increase in the strength of the composite over the PUU-only film, with increasing MOF (Table 1). The UiO-66/PUU MMMs had high toughness when compared to the UiO-66/PVDF MMMs. In two cases, the 20 and 30 wt % MMMs, the MMM had toughness (>140 J/cm³) that may provide a good balance of mechanical properties and protection (Table S2). The tensile testing illustrates that UiO-66/PUU MMMs are strong, ductile materials.

MOF/PUU MMMs for CWA Simulant Degradation. With confirmation that MOF/PUU composites are strong and flexible, these materials were tested for catalytic activity related to their desired protective function. To assess the activity of the MMMs for the breakdown of organophosphorous nerve agents, a well-studied, less toxic simulant molecule dimethyl-4-nitrophenylphosphate (DMNP) was used. Using a previously developed method, the samples were analyzed in triplicate and were monitored simultaneously in a 24-well plate format using a plate reader at pH = 8.0. Using a plate format using

A variety of MOF-PUU composites were tested for DMNP hydrolysis including composites with increasing MOF loading (20, 30, and 50 wt %) and differing MOF functionalization (UiO-66, UiO-66-NH₂, UiO-66-NO₂, and UiO-66-Naph). The MOF/PUU MMMs successfully degraded the simulant, indicating that the MOF is chemically accessible despite showing no N₂ gas sorption (see above).⁴² As expected, increased MOF loading increases the hydrolysis rate (Table S4 and Figure S15). MMMs made with the functionalized MOF (50 wt %) were also tested and showed variations in hydrolysis activities (Table S4 and Figure S16). The activities of PUU MMMs do not correlate with the activities of the assynthesized MOF powders. For example, UiO-66 and UiO-66-NO₂ show comparable activities as powders, but the UiO-66/PUU MMM has a 6-fold faster rate than the UiO-66-NO₂/ PUU MMM. Also, the UiO-66-NH2 PUU MMM has the highest hydrolysis rate despite the as-synthesized MOF powder

being much slower than UiO-66 and UiO-66-NO₂ powders. Deviations in properties for powder MOFs versus MOF—polymer composites have been observed in gas sorption studies. Here, MOF ligand functionality is found to affect the catalytic rate of a composite; although the origins of this effect are unclear at this time, it does provide a possible avenue for further study and optimization.

PUU-based MMMs of 50 wt % UiO-66 and UiO-66-NH₂ were compared with analogous PVDF MMMs for DMNP hydrolysis. Interestingly, the UiO-66 and UiO-66-NH₂ PVDF MMMs do correlate in activity to the reported hydrolysis rates of the pure MOF powders (Figures S16 and S17 and Table S4). This suggests that the selection of both the polymer and the MOF affects the performance of the resulting composite. For UiO-66 and UiO-66-NH₂, properties such as the particle size (128 \pm 29 and 199 \pm 48 nm, respectively), morphology by SEM, and mechanical properties of the resulting MMMs by tensile testing are similar, suggesting that other factors influence the resulting reactivity of the composites.

The MOF–polymer interface is an important factor for understanding the composite behavior. A number of studies have focused on understanding this interface using molecular dynamics (MD) simulations, ^{45–47} focused ion beam-milled SEM, ^{45,48} and solid-state NMR (SSNMR). ⁴⁷ MOF-based MMMs with PVDF and poly(ethylene oxide) (PEO) have been previously shown to have very different MOF–polymer interfaces using MD and SSNMR, ⁴⁷ and these MMMs also show large differences in DMNP hydrolysis. ²² While in-depth interface studies are outside the scope of this work, differences in these interfaces may explain the variations in DMNP reactivity observed here.

Despite limitations in our understanding of the origin of DMNP hydrolysis in these MOF–polymer composites, the ability to screen a large number of composites (12 in this study) using the parallel screening method does enable the identification of improved MOF–polymer combinations. In the case of 50 wt % UiO-66-NH₂/PUU, the rate is almost equal to the PVDF MMMs and previously reported cross-linked polythiourea-UiO-66-NH₂-coated fabrics reported under similar assay conditions. However, the mechanical properties of the PUU composites are far superior to the PVDF composites, making it more suited to practical uses in PPE.

MOF/PUU Fibers. Spandex is typically used as woven materials from melt or wet spun fibers and incorporating MOFs into this process is important for applications in protective equipment. To test the viability of these composites in their anticipated form factor, 50 wt % UiO-66 and UiO-66-NH₂/PUU fibers were drawn using a rudimentary wet spinning apparatus. Continuous fibers >3 m were made with phase inversion of the DMAC-based ink into a water bath and manually drawing the fiber. Despite being 50 wt % crystalline MOF (Figures S18-S20), the fiber can be manipulated and stretched (Video S5). Figure 5 illustrates the practical handling of the fiber with a simple knot and weave that can be done without fracture. The preparation method also results in a more porous microstructure of the composite due to the nonsolvent contact in the drawing step (Figures 5, S21, and S22). This proof-of-concept demonstrates that with optimization of fiber processing, MOF-based PUU fibers are viable.

The fibrous, porous structure introduced into the composite affects the properties of the fiber composite compared to the

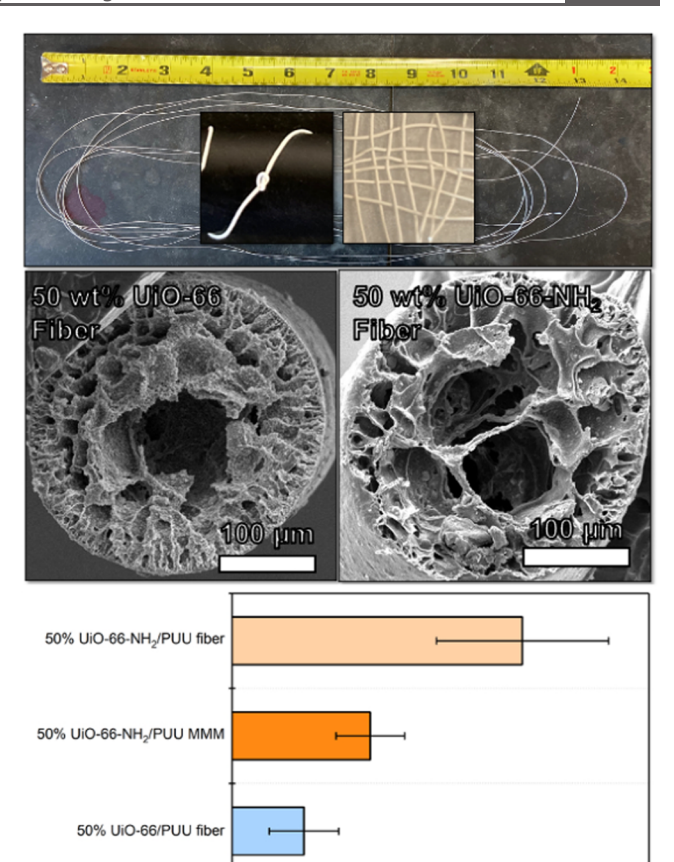


Figure 5. Top: photographs of a single 3 m strand, knotted section, and woven threads of 50 wt % UiO-66/PUU fibers. Center: cross-sectional SEM images of 50 wt % MOF/PUU fibers. Bottom: DMNP hydrolysis rates for MOF/PUU MMMs and fibers, normalized by the mass of the composite.

DMNP Hydrolysis Rate (mM \times sec⁻¹ \times mg⁻¹ \times 10⁻⁶)

50% UiO-66/PUU MMM

equivalent MMM. The ductility of 50 wt % UiO-66/PUU fibers remains similar to that of MMM (elongations at break of 122 and 146%, respectively), but the strength is reduced by an order of magnitude (ultimate tensile strengths of 1.02 and 9.53 MPa, respectively) (Table S2 and Figure S23). The same trend holds true for 50 wt % UiO-66-NH $_2$ /PUU fibers and MMMs (Table S2 and Figure S24). The porous morphology of the fibers likely led to the reduction in mechanical properties. Despite the lowering of strength, the 50 wt % UiO-66/PUU fiber still had a higher toughness than the 50 wt % UiO-66/PVDF MMM.

To test these composites for gas uptake, a 50 wt % UiO-66-NH₂/PUU fiber was evaluated for $\rm CO_2$ sorption. Unlike the N₂ sorption isotherms collected at 77 K for the MMM, the $\rm CO_2$ isotherms were collected at 295 K. These fibers adsorb $\rm CO_2$ with ~28% of the latent MOF porosity accessible to the gas (Table S5 and Figure S25). This room temperature sorption experiment demonstrates that these composites possess accessible porosity under ambient conditions.

The new fiber form factor was also tested in the DMNP hydrolysis assay. With the porous nature of the fiber, the transport of DMNP was improved, as better activity was

observed on a per MOF weight basis in composites of both UiO-66 and UiO-66-NH $_2$ (Figures 5 and S15). This effect was most pronounced in UiO-66-NH $_2$ where the rate almost doubles when in the fiber (Figure 5). This increase in the hydrolysis rate indicates that the form factor of the MOF—polymer composite is an important consideration for use in PPF.

MOF/PUU Electrospun Nanofibers. While PUU/MOF composites were successfully processed into fiber form using wet spinning, the relatively large diameter of these fibers may limit their use in certain applications. Therefore, the potential for processing nanofibers via electrospinning was explored. Nanofiber-based composites are often used in filtration applications for the removal of aerosols, and the incorporation of MOFs can aid in the filtration of toxic chemicals and pollutants. ^{28,50}

Electrospinning of PUU-based composites was conducted to showcase the versatility of the materials using a variety of processing techniques. To a 10 wt % PUU electrospinning solution in DMF was added a suitable amount of the MOF to achieve a 20 wt % MOF content in the final composite. SEM images for nanofibers electrospun from both UiO-66 and UiO-66-NH₂ are shown in Figure 6. Fibers produced from

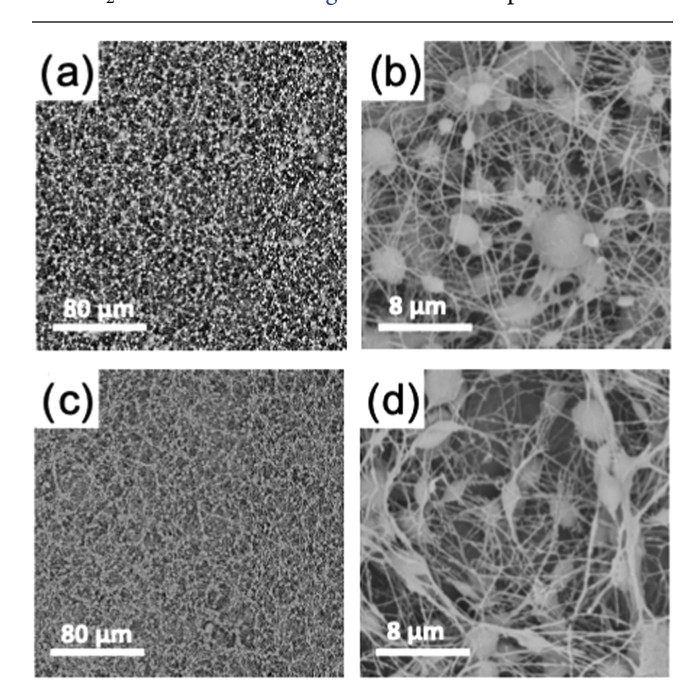


Figure 6. SEM images of 20 wt % UiO-66/PUU electrospun nanofiber composites magnified at: (a) $1000\times$ and (b) $10\,000\times$. 20 wt % UiO-66-NH₂/PUU electrospun nanofiber composites magnified at: (c) $1000\times$ and (d) $10\,000\times$.

electrospinning exhibited good dispersion of MOFs throughout the mat. ThermoFisher Phenom FiberMetric software was used to estimate fiber diameters of the composite, and the average fiber diameters for the materials were calculated to be $\sim\!350\pm150$ and $\sim\!425\pm160$ nm for UiO-66/PUU and UiO-66-NH₂/PUU, respectively (Figures S26 and S27). The MOFs remained intact throughout the electrospinning process as evidenced by PXRD (Figure S28). The ability of this composite to be electrospun into nanofibers adds to the versatility of MOF/PUU materials for PPE applications.

To demonstrate the utility of this fabrication method, the 20 wt % UiO-66/PUU electrospun nanofiber mats were tested for DMNP hydrolysis. Using the same methods for monitoring hydrolysis for the MMMs and fibers, the electrospun mat had a DMNP hydrolysis rate of 9.4 \pm 1.8 mM \times sec $^{-1}$ \times mg $^{-1}$ \times 10 $^{-6}$. The 20 wt % electrospun composite has a rate similar to that of the 50 wt % MMM (Figure S29). This result highlights the potential utility of MOF/PUU composites even at relatively low MOF loadings. This data further demonstrates that form factors can account for differences in the hydrolysis rate.

CONCLUSIONS

A new spandex-like MOF composite was developed with a focus on developing materials with the mechanical properties necessary for use in active PPE. The resulting MOF/PUU composites showed high strength and flexibility. A range of MOF loadings allowed for the tailoring of ductility and tensile strength in the resulting composites. These materials are highly active to nerve agent simulant hydrolysis and the rate depends on the MOF content, polymer, and form factor of the composite. MOF/PUU fibers and electrospun mats indicate that these composites are versatile and can be engineered into form factors other than simple films.

ASSOCIATED CONTENT

Supporting Information

The Supporting Information is available free of charge at https://pubs.acs.org/doi/10.1021/acs.chemmater.0c04874.

Videos demonstrating the handling of MOF-polymer composite. Detailed materials and experimental procedures; polymer synthetic scheme; gel-permeation chromatograph; gas sorption results; photographs of composites; SEM images; PXRD patterns; tensile testing results; and DMNP hydrolysis results (PDF)

AUTHOR INFORMATION

Corresponding Author

Seth M. Cohen — Department of Chemistry and Biochemistry, University of California, San Diego, La Jolla, California 92093, United States; Department of Nanoengineering, University of California, San Diego, Jacobs School of Engineering, La Jolla, California 92093, United States; orcid.org/0000-0002-5233-2280; Email: scohen@ucsd.edu

Authors

Joseph M. Palomba – Department of Chemistry and Biochemistry, University of California, San Diego, La Jolla, California 92093, United States

David M. Wirth – Department of Nanoengineering, University of California, San Diego, Jacobs School of Engineering, La Jolla, California 92093, United States

Jin Yeong Kim − Department of Chemistry and Biochemistry, University of California, San Diego, La Jolla, California 92093, United States; o orcid.org/0000-0003-2250-8780

Mark Kalaj — Department of Chemistry and Biochemistry, University of California, San Diego, La Jolla, California 92093, United States; oorcid.org/0000-0001-7139-7517

Evan M. Clarke – Department of Chemistry and Biochemistry, University of California, San Diego, La Jolla, California 92093, United States

Gregory W. Peterson – DEVCOM Chemical and Biological Center, U.S. Army, Aberdeen Proving Ground, Maryland 21020, United States; orcid.org/0000-0003-3467-5295

Jonathan K. Pokorski – Department of Nanoengineering, University of California, San Diego, Jacobs School of Engineering, La Jolla, California 92093, United States

Complete contact information is available at: https://pubs.acs.org/10.1021/acs.chemmater.0c04874

Notes

The authors declare no competing financial interest.

ACKNOWLEDGMENTS

This work was supported by the Department of Army Research under grant number W911NF-20-2-0143 and the Joint Science and Technology Office for Chemical and Biological Defense (JSTO-CBD) under project CB3934. J.M.P. was supported by the USD/R&E (the Under Secretary of Defense-Research and Engineering), National Defense Education Program (NDEP)/ BA-1, and Basic Research in the Science Mathematics and Research for Transformation (SMART) Scholarship Program. J.K.P. and D.M.W acknowledged funding from the National Science Foundation (OISE 1844463). This work was performed in part at the San Diego Nanotechnology Infrastructure (SDNI) of U.C. San Diego, a member of the National Nanotechnology Coordinated Infrastructure, which was supported by the National Science Foundation (Grant ECCS-1542148). M.K. was supported by the Department of Defense (DoD) through the National Defense Science and Engineering Graduate (NDSEG) Fellowship Program and is the recipient of an Achievement Rewards for College Scientists (ARCS) Foundation Fellowship. The authors would like to thank Zhaoqiang Song for helping with tensile testing experiments and Dr. Brian R. Pimentel, Dr. Jessica C. Moreton, Dr. Sergio Ayala Jr., and Dr. Kathleen E. Prosser for helpful discussions.

REFERENCES

- (1) Kalaj, M.; Bentz, K. C.; Ayala, S.; Palomba, J. M.; Barcus, K. S.; Katayama, Y.; Cohen, S. M. MOF-Polymer Hybrid Materials: From Simple Composites to Tailored Architectures. *Chem. Rev.* **2020**, *120*, 8267–8302.
- (2) Kirlikovali, K. O.; Chen, Z.; Islamoglu, T.; Hupp, J. T.; Farha, O. K. Zirconium-Based Metal—Organic Frameworks for the Catalytic Hydrolysis of Organophosphorus Nerve Agents. *ACS Appl. Mater. Interfaces* **2020**, *12*, 14702—14720.
- (3) Bobbitt, N. S.; Mendonca, M. L.; Howarth, A. J.; Islamoglu, T.; Hupp, J. T.; Farha, O. K.; Snurr, R. Q. Metal—organic frameworks for the removal of toxic industrial chemicals and chemical warfare agents. *Chem. Soc. Rev.* **2017**, *46*, 3357–3385.
- (4) Furukawa, H.; Cordova, K. E.; O'Keeffe, M.; Yaghi, O. M. The Chemistry and Applications of Metal-Organic Frameworks. *Science* **2013**, *341*, No. 1230444.
- (5) Yuan, S.; Feng, L.; Wang, K.; Pang, J.; Bosch, M.; Lollar, C.; Sun, Y.; Qin, J.; Yang, X.; Zhang, P.; Wang, Q.; Zou, L.; Zhang, Y.; Zhang, L.; Fang, Y.; Li, J.; Zhou, H.-C. Stable Metal—Organic Frameworks: Design, Synthesis, and Applications. *Adv. Mater.* **2018**, *30*, No. 1704303.
- (6) DeCoste, J. B.; Peterson, G. W. Metal-Organic Frameworks for Air Purification of Toxic Chemicals. *Chem. Rev.* **2014**, *114*, 5695–5727.
- (7) Islamoglu, T.; Chen, Z.; Wasson, M. C.; Buru, C. T.; Kirlikovali, K. O.; Afrin, U.; Mian, M. R.; Farha, O. K. Metal–Organic Frameworks against Toxic Chemicals. *Chem. Rev.* **2020**, *120*, 8130–8160.

- (8) Bandosz, T. J.; Laskoski, M.; Mahle, J.; Mogilevsky, G.; Peterson, G. W.; Rossin, J. A.; Wagner, G. W. Reactions of VX, GD, and HD with Zr(OH)4: Near Instantaneous Decontamination of VX. J. Phys. Chem. C 2012, 116, 11606–11614.
- (9) Wagner, G. W.; Procell, L. R.; O'Connor, R. J.; Munavalli, S.; Carnes, C. L.; Kapoor, P. N.; Klabunde, K. J. Reactions of VX, GB, GD, and HD with Nanosize Al2O3. Formation of Aluminophosphonates. J. Am. Chem. Soc. 2001, 123, 1636–1644.
- (10) Wagner, G. W.; Bartram, P. W. Reactions of VX, HD, and Their Simulants with NaY and AgY Zeolites. Desulfurization of VX on AgY. *Langmuir* **1999**, *15*, 8113–8118.
- (11) Jung, D.; Das, P.; Atilgan, A.; Li, P.; Hupp, J. T.; Islamoglu, T.; Kalow, J. A.; Farha, O. K. Reactive Porous Polymers for Detoxification of a Chemical Warfare Agent Simulant. *Chem. Mater.* **2020**, *32*, 9299–9306
- (12) DeCoste, J. B.; Demasky, T. J.; Katz, M. J.; Farha, O. K.; Hupp, J. T. A UiO-66 analogue with uncoordinated carboxylic acids for the broad-spectrum removal of toxic chemicals. *New J. Chem.* **2015**, *39*, 2396–2399.
- (13) Katz, M. J.; Mondloch, J. E.; Totten, R. K.; Park, J. K.; Nguyen, S. T.; Farha, O. K.; Hupp, J. T. Simple and Compelling Biomimetic Metal—Organic Framework Catalyst for the Degradation of Nerve Agent Simulants. *Angew. Chem.* **2014**, *126*, 507—511.
- (14) Plonka, A. M.; Wang, Q.; Gordon, W. O.; Balboa, A.; Troya, D.; Guo, W.; Sharp, C. H.; Senanayake, S. D.; Morris, J. R.; Hill, C. L.; Frenkel, A. I. In Situ Probes of Capture and Decomposition of Chemical Warfare Agent Simulants by Zr-Based Metal Organic Frameworks. J. Am. Chem. Soc. 2017, 139, 599–602.
- (15) Palomba, J. M.; Credille, C. V.; Kalaj, M.; DeCoste, J. B.; Peterson, G. W.; Tovar, T. M.; Cohen, S. M. High-throughput screening of solid-state catalysts for nerve agent degradation. *Chem. Commun.* **2018**, *54*, 5768–5771.
- (16) Peterson, G. W.; DeCoste, J. B.; Fatollahi-Fard, F.; Britt, D. K. Engineering UiO-66-NH2 for Toxic Gas Removal. *Ind. Eng. Chem. Res.* **2014**, 53, 701–707.
- (17) DeCoste, J. B.; Browe, M. A.; Wagner, G. W.; Rossin, J. A.; Peterson, G. W. Removal of chlorine gas by an amine functionalized metal—organic framework via electrophilic aromatic substitution. *Chem. Commun.* **2015**, *51*, 12474—12477.
- (18) Liu, Y.; Howarth, A. J.; Vermeulen, N. A.; Moon, S.-Y.; Hupp, J. T.; Farha, O. K. Catalytic degradation of chemical warfare agents and their simulants by metal-organic frameworks. *Coord. Chem. Rev.* **2017**, 346, 101–111.
- (19) Kalaj, M.; Denny, M. S., Jr; Bentz, K. C.; Palomba, J. M.; Cohen, S. M. Nylon–MOF Composites through Postsynthetic Polymerization. *Angew. Chem., Int. Ed.* **2019**, *58*, 2336–2340.
- (20) Zhao, J.; Lee, D. T.; Yaga, R. W.; Hall, M. G.; Barton, H. F.; Woodward, I. R.; Oldham, C. J.; Walls, H. J.; Peterson, G. W.; Parsons, G. N. Ultra-Fast Degradation of Chemical Warfare Agents Using MOF—Nanofiber Kebabs. *Angew. Chem., Int. Ed.* **2016**, *55*, 13224—13228.
- (21) Peterson, G. W.; Lu, A. X.; Hall, M. G.; Browe, M. A.; Tovar, T.; Epps, T. H. MOFwich: Sandwiched Metal—Organic Framework-Containing Mixed Matrix Composites for Chemical Warfare Agent Removal. ACS Appl. Mater. Interfaces 2018, 10, 6820—6824.
- (22) Ma, K.; Islamoglu, T.; Chen, Z.; Li, P.; Wasson, M. C.; Chen, Y.; Wang, Y.; Peterson, G. W.; Xin, J. H.; Farha, O. K. Scalable and Template-Free Aqueous Synthesis of Zirconium-Based Metal—Organic Framework Coating on Textile Fiber. *J. Am. Chem. Soc.* **2019**, *141*, 15626–15633.
- (23) Liang, H.; Yao, A.; Jiao, X.; Li, C.; Chen, D. Fast and Sustained Degradation of Chemical Warfare Agent Simulants Using Flexible Self-Supported Metal—Organic Framework Filters. *ACS Appl. Mater. Interfaces* **2018**, *10*, 20396–20403.
- (24) Barton, H. F.; Davis, A. K.; Parsons, G. N. The Effect of Surface Hydroxylation on MOF Formation on ALD Metal Oxides: MOF-525 on TiO2/Polypropylene for Catalytic Hydrolysis of Chemical Warfare Agent Simulants. ACS Appl. Mater. Interfaces 2020, 12, 14690–14701.

- (25) Denny, M. S.; Kalaj, M.; Bentz, K. C.; Cohen, S. M. Multicomponent metal—organic framework membranes for advanced functional composites. *Chem. Sci.* **2018**, *9*, 8842—8849.
- (26) DeCoste, J. B.; Denny, J. M. S.; Peterson, G. W.; Mahle, J. J.; Cohen, S. M. Enhanced aging properties of HKUST-1 in hydrophobic mixed-matrix membranes for ammonia adsorption. *Chem. Sci.* **2016**, *7*, 2711–2716.
- (27) Wang, S.; Pomerantz, N. L.; Dai, Z.; Xie, W.; Anderson, E. E.; Miller, T.; Khan, S. A.; Parsons, G. N. Polymer of intrinsic microporosity (PIM) based fibrous mat: combining particle filtration and rapid catalytic hydrolysis of chemical warfare agent simulants into a highly sorptive, breathable, and mechanically robust fiber matrix. *Mater. Today Adv.* **2020**, *8*, No. 100085.
- (28) Peterson, G. W.; Lu, A. X.; Epps, T. H. Tuning the Morphology and Activity of Electrospun Polystyrene/UiO-66-NH2 Metal—Organic Framework Composites to Enhance Chemical Warfare Agent Removal. ACS Appl. Mater. Interfaces 2017, 9, 32248–32254.
- (29) Kim, K.; Seo, J. Y.; Baek, K.-Y.; Bae, J.-Y.; Shin, S. Metalorganic framework (UiO-66)-dispersed polyurethane composite films for the decontamination of methyl paraoxon. *Polym. Int.* **2019**, *68*, 1502–1508.
- (30) Mahdi, E. M.; Tan, J.-C. Dynamic molecular interactions between polyurethane and ZIF-8 in a polymer-MOF nanocomposite: Microstructural, thermo-mechanical and viscoelastic effects. *Polymer* **2016**, *97*, 31–43.
- (31) Smith, Z. P.; Bachman, J. E.; Li, T.; Gludovatz, B.; Kusuma, V. A.; Xu, T.; Hopkinson, D. P.; Ritchie, R. O.; Long, J. R. Increasing M2(dobdc) Loading in Selective Mixed-Matrix Membranes: A Rubber Toughening Approach. *Chem. Mater.* **2018**, *30*, 1484–1495.
- (32) Peterson, G. W.; Au, K.; Tovar, T. M.; Epps, T. H. Multivariate CuBTC Metal—Organic Framework with Enhanced Selectivity, Stability, Compatibility, and Processability. *Chem. Mater.* **2019**, *31*, 8459—8465.
- (33) Singha, K. Analysis of Spandex/Cotton Elastomeric Properties: Spinning and Applications. *Int. J. Compos. Mater.* **2012**, *2*, 11–16.
- (34) Denny, M. S., Jr; Cohen, S. M. In Situ Modification of Metal—Organic Frameworks in Mixed-Matrix Membranes. *Angew. Chem., Int. Ed.* **2015**, *54*, 9029–9032.
- (35) Duan, P.; Moreton, J. C.; Tavares, S. R.; Semino, R.; Maurin, G.; Cohen, S. M.; Schmidt-Rohr, K. Polymer Infiltration into Metal—Organic Frameworks in Mixed-Matrix Membranes Detected in Situ by NMR. J. Am. Chem. Soc. 2019, 141, 7589—7595.
- (36) Sakurai, S.; Okamoto, Y.; Sakaue, H.; Nakamura, T.; Banda, L.; Nomura, S. Structure and properties of segmented poly-(urethaneurea)s with relatively short hard-segment chains. *J. Polym. Sci. B* **2000**, *38*, 1716–1728.
- (37) Korinko, P.; Chapman, G. Characterization Of Tensile Strength Of Glovebox Gloves; 2012; p 28.
- (38) Rego, A.; Roley, L. In-use barrier integrity of gloves: Latex and nitrile superior to vinyl. *Am. J. Infect. Control* **1999**, 27, 405–410.
- (39) Wu, S. Phase structure and adhesion in polymer blends: A criterion for rubber toughening. *Polymer* **1985**, *26*, 1855–1863.
- (40) Kalaj, M.; Palomba, J. M.; Bentz, K. C.; Cohen, S. M. Multiple functional groups in UiO-66 improve chemical warfare agent simulant degradation. *Chem. Commun.* **2019**, *55*, 5367–5370.
- (41) Moreton, J. C.; Denny, M. S.; Cohen, S. M. High MOF loading in mixed-matrix membranes utilizing styrene/butadiene copolymers. *Chem. Commun.* **2016**, *52*, 14376–14379.
- (42) Moreton, J. C.; Palomba, J. M.; Cohen, S. M. Liquid-Phase Applications of Metal—Organic Framework Mixed-Matrix Membranes Prepared from Poly(ethylene-co-vinyl acetate). *ACS Appl. Polym. Materials* **2020**, *2*, 2063—2069.
- (43) Peterson, G. W.; Wang, H.; Au, K.; Epps, T. H., III Metal-Organic Framework-Polymer Composite Enhancement via Acyl Chloride Modification. *Polym. Inter.* **2020**, DOI: 10.1002/pi.6151.
- (44) Ma, L.; Svec, F.; Lv, Y.; Tan, T. Engineering of the Filler/Polymer Interface in Metal-Organic Framework-Based Mixed-Matrix Membranes to Enhance Gas Separation. *Chem. Asian J.* **2019**, *14*, 3502–3514.

- (45) Vornholt, S. M.; Duncan, M. J.; Warrender, S. J.; Semino, R.; Ramsahye, N. A.; Maurin, G.; Smith, M. W.; Tan, J.-C.; Miller, D. N.; Morris, R. E. Multifaceted Study of the Interactions between CPO-27-Ni and Polyurethane and Their Impact on Nitric Oxide Release Performance. ACS Appl. Mater. Interfaces 2020, 12, 58263–58276.
- (46) Semino, R.; Moreton, J. C.; Ramsahye, N. A.; Cohen, S. M.; Maurin, G. Understanding the origins of metal—organic framework/polymer compatibility. *Chem. Sci.* **2018**, *9*, 315–324.
- (47) Duan, P.; Moreton, J. C.; Tavares, S. R.; Semino, R.; Maurin, G.; Cohen, S. M.; Schmidt-Rohr, K. Polymer Infiltration into Metal—Organic Frameworks in Mixed-Matrix Membranes Detected in Situ by NMR. J. Am. Chem. Soc. 2019, 141, 7589—7595.
- (48) Rodenas, T.; Luz, I.; Prieto, G.; Seoane, B.; Miro, H.; Corma, A.; Kapteijn, F.; Llabrés i Xamena, F. X.; Gascon, J. Metal—organic framework nanosheets in polymer composite materials for gas separation. *Nature Mater.* **2015**, *14*, 48–55.
- (49) Kalaj, M.; Cohen, S. M. Spray-Coating of Catalytically Active MOF-Polythiourea through Postsynthetic Polymerization. *Angew. Chem., Int. Ed.* **2020**, *59*, 13984–13989.
- (50) Zhang, Y.; Yuan, S.; Feng, X.; Li, H.; Zhou, J.; Wang, B. Preparation of Nanofibrous Metal—Organic Framework Filters for Efficient Air Pollution Control. *J. Am. Chem. Soc.* **2016**, *138*, 5785—5788